

A NUMERICAL STUDY OF THE EFFECTS OF LEADING EDGE
VORTEX FLAPS ON THE PERFORMANCE OF A 75° DELTA WING

by

Mary Ellen McNutt

Thesis submitted to the Faculty of the
Virginia Polytechnic Institute and State University
in partial fulfillment of the requirements for the degree of
MASTER OF SCIENCE
in
Aerospace Engineering

APPROVED:

~~Chairman, Prof. J. F. Marchman, III~~

Prof. J. A. Schetz

Prof. F. H. Lutze

January, 1982
Blacksburg, Virginia

ACKNOWLEDGMENTS

I would like to thank Professor J. F. Marchman for his guidance and assistance. I would also like to thank Professor J. A. Schetz and Professor F. H. Lutze for serving on my graduate committee.

Thanks also go to Professor Dean T. Mook and Takis Konstadinopoulos of the Engineering Science and Mechanics Department who provided the initial program on which this work is based. I am also grateful to James F. Campbell and Neal Frink of the NASA Langley Research Center who provided valuable insight during the course of this work.

TABLE OF CONTENTS

	<u>Page</u>
ACKNOWLEDGMENTS	ii
LIST OF FIGURES	iv
CHAPTER ONE. INTRODUCTION	1
CHAPTER TWO. LITERATURE REVIEW	4
2.1 Experimental Investigations	4
2.2 Analytical Methods	6
2.3 Discrete Vortex Methods	7
CHAPTER THREE. STATEMENT OF PROBLEM AND METHOD OF SOLUTION . .	9
3.1 Problem Statement	9
3.2 The Basic Method	9
3.3 Lattice Arrangement	12
3.4 Method of Solution	13
3.5 Calculation of Loads	13
3.6 Notes on Convergence and Computer Times	17
CHAPTER FOUR. NUMERICAL RESULTS	18
CHAPTER FIVE. CONCLUSIONS AND RECOMMENDATIONS	22
REFERENCES	23
FIGURES	26
VITA	48

LIST OF FIGURES

<u>Table</u>		<u>Page</u>
1	Calculation times for various configurations	26
<u>Figure</u>		
1	Flow field over a delta wing with leading edge separation	27
2	Resultant force on various leading edges	28
3	Nonlinear aspect of aerodynamic loads on wings with vortex lift	29
4	Biot-Savart law	30
5	Shed vortex lines	31
6	Vortex lattice	32
7	Definitions for calculations of loads using Bernoulli's equation	33
8	Pressure distribution - flat delta $\alpha = 10^\circ$	34
9	Pressure distribution - flat delta $\alpha = 20^\circ$	35
10	Pressure distribution - flat delta $\alpha = 30^\circ$	36
11	Pressure distribution - leading edge flap, $\alpha = 10^\circ$	37
12	Pressure distribution - leading edge flap, $\alpha = 20^\circ$	38
13	Pressure distribution - leading edge flap	39
14	Leading edge and trailing edge wakes on a flat delta, $\alpha = 15^\circ$	40
15	Leading edge and trailing edge wakes on a delta with 30° leading edge flap, $\alpha = 15^\circ$	41
16	Lift coefficient vs angle of attack - no flap	42
17	Lift coefficient vs angle of attack - 30° leading edge flap	43

<u>Figure</u>		<u>Page</u>
18	Lift coefficient vs angle of attack - plain wing and leading edge flap	44
19	Axial force coefficient vs $\sin^2\alpha$	45
20	Drag coefficient vs lift coefficient	46
21	Pitching moment coefficient vs angle of attack . . .	47

Chapter One

INTRODUCTION

The past twenty years have seen dramatic changes in aircraft wing design. Among these have been the use of delta and other highly swept wings which utilize low aspect ratios and sharp leading edges to achieve efficient supersonic cruise. Because of this, they are inefficient at low subsonic speeds encountered during take-off, landing and maneuvers. Flow separation occurs along the sharp leading edge of the wing resulting in the formation of a vortex above the wing surface. The strong spanwise component of the velocity generated by this vortex produces a pressure gradient which reattaches the flow over the wing's upper surface. The flow field is depicted in Figure 1. The result is an increase in lift but also an increase in drag due to the orientation of the resultant force produced by the vortex, as shown in Figure 2a. Hence the aerodynamic loads on a low aspect ratio wing at high angles of attack are strongly non-linear functions of angle of attack. See Figure 3.

The vortex flow on the wing is very sensitive to changes in the free stream flow. At high angles of attack and in certain yawed configurations, vortex bursting occurs, resulting in a drastic reduction of lift. Changes in vortex core location move the center of pressure on the wing causing pitch stability problems. There are several ways to stabilize the vortex location and prevent vortex bursting. Among these are the use of spanwise blowing, the addition of leading edge

camber by reshaping the wing itself, or the use of leading edge vortex flaps. On the moderately swept wings typical of fighter aircraft, spanwise blowing holds promise for enhancing vortex flow. An account of the spanwise blowing concept can be found in the work of Campbell¹. The use of a cambered leading edge prevents leading edge separation and vortex formation as shown in Figure 2b. Hence this approach reduces the drag but also causes the loss of some lift. It is also effective in stabilizing pitching moment at high angles of attack. However, these benefits may be outweighed by reductions in overall supersonic performance due to the cambered shape.

The vortex flap controls the flow by causing the vortex to form on the flap. Ideally, the flow reattaches at the wing-flap hinge line providing attached flow over the entire wing. The force produced by the vortex is now oriented to provide a leading edge thrust shown in Figure 2c. Overall stability is increased by confining the vortex to the flap.

Various numerical codes have been developed to predict the aerodynamic loads on wings with vortex flow. The fastest, and hence most economical, methods^{2,3} predict only loads with no detailed pressure distributions. At the other extreme, the most complete method thus far, the Free Vortex Sheet code developed by the Boeing Company under NASA contract^{4,5} gives detailed pressure information at the expense of long computer times required for solution. The present work utilizes a general, unsteady, subsonic, nonlinear, vortex lattice method which gives pressure distributions and loads using relatively short computer times. Thus the aerodynamic loads and pressure distributions on a

delta wing, with and without leading edge flaps, are found by using a relatively quick method.

Chapter Two

LITERATURE REVIEW

The review of pertinent literature is divided into three sections, experimental investigations, analytical methods, and discrete vortex methods.

2.1 Experimental Investigations

As early as 1937 Winter⁶ found that the aerodynamic loads of a low aspect ratio wing were nonlinear functions of angle of attack. Whittle and Lovell⁷ observed the vortex flow over a 60° delta wing with a 10 percent biconvex section and tested the effects of semispan and full span leading edge and trailing edge flaps. They found that a 30° deflection of the full span leading edge flaps produced the largest increase in $C_{L_{max}}$, from 1.08 to 1.22, while at the same time reducing drag and affecting pitching moment only negligibly. Also they observed that the results did not depend on Reynolds number.

Bartlett and Vidal⁸ looked at the effects of edge shape on various low aspect ratio wings. They found that wings with sharp edges showed no variation with changing Reynolds number since the flow separated at the leading edge regardless of the nature of the boundary layer. However, wings with rounded edges showed a slight variation with Reynolds number. Overall, sharp edges yielded higher lift coefficients, more negative pitching moments, and higher drag coefficients.

Peckham⁹ tested a wide range of uncambered delta and gothic wings with varying thicknesses. He observed primary and secondary separation

lines along the leading edges and found that the effect of increasing thickness or increasing aspect ratio was to move the attachment line and peak suction line further outboard on the wing. Increasing thickness also caused reduction in lift and a more negative pitching moment, thereby implying a loss of lift over the forward part of the wing. Conversely, increasing aspect ratio increased lift and increased pitching moment (to less negative values). He noted that a possible method for increasing lift coefficient would be the employment of a 'leading edge flap' which could be extended for take-off and landing to effectively increase the aspect ratio. Further, he observed the extreme sensitivity of vortex breakdown to even small yaw angles for the wing without a flap extension.

Wentz¹⁰ conducted tests on a 74° delta with conical camber, apex camber, and constant percent chord leading edge flaps at different deflection angles. He concluded that leading edge camber had only a slight effect on total lift while reducing drag due to lift at high angles. Leading edge camber was found to have large effect on pitching moment characteristics, with camber near the apex being most effective in improving the pitch stability of the wing. The leading edge flap showed improvements in drag and pitching moment similar to the apex cambered model.

Several configurations of leading edge flaps with different hinge lines and with trailing edge flaps were tested by Rao¹¹ on a 74° delta wing. He found that, with increasing angle of attack, the flaps caused a forward movement along the flap of the vortex location, producing a longitudinal shift of the center of pressure. So that, below 10°, the

flaps reduced stability by increasing the slope of the pitching moment curve due to the added flap area forward of the moment center. At higher angles of attack, with the entire length of the flap under vortex flow, pitch stability improved as the slope of the pitching moment curve was decreased until it reached the same value as that of the plain wing. The overall best flap was judged to be an inverse tapered flap which started at 25 percent of the leading edge length from the apex, with 15 percent wing area and a mean chord approximately 5 percent \bar{c} of the wing. At the optimum deflection angle of 30° , there was a 30 to 40 percent decrease in drag.

Marchman¹² investigated various constant chord leading edge flaps on 60° and 75° delta wings. Again, while nominal changes in lift were observed, substantial reductions, up to 40 percent, in drag were found at moderate angles of attack for both wings. Flaps with 38 percent wing area deflected at 30° were determined to give optimum results. Pitching moment was adversely affected by the flaps, with both wings exhibiting unstable behavior at higher angles of attack. A tapered flap, with zero chord at the apex, was found to be more stable while still reducing drag substantially.

2.2 Analytical Methods

Of the analytical methods, the leading edge suction analogy is the most widely used. Polhamus^{13,14} developed the method to predict lift and drag for sharp edged delta and delta related wings. It accurately predicts the loads on thin wings with no camber or twist. The method is based on the assumption that if flow reattachment occurs on the

upper surface of the wing, then the total lift can be calculated as the sum of a potential flow lift and a vortex flow lift.

$$C_{L_T} = C_{L_P} + C_{L_V}$$

When separation is fixed at the leading edge, there is no leading edge suction developed and the potential lift term is found by using the Kutta-Joukowski theorem. Thus,

$$C_{L_P} = K_p \sin \alpha \cos^2 \alpha$$

where K_p is the normal force slope given by potential theory and dependent only on planform.

Since flow reattachment occurs on the upper surface of the wing, there must be a normal force which maintains the equilibrium of the flow. This normal force is equal to the theoretical leading edge suction force, C_{sp} . The expression for the vortex lift is given by

$$C_{L_V} = K_V \cos \alpha \sin^2 \alpha$$

where $K_V = \partial C_{sp} / \partial \alpha^2$. The drag coefficient due to lift is found using

$$C_D = C_L \tan \alpha = K_p \sin^2 \alpha \cos \alpha + K_V \sin^3 \alpha$$

Polhamus' method accurately predicts the total lift and drag but cannot predict pitching moment or wake shape.

2.3 Discrete Vortex Methods

The earliest attempts to develop an analytical method to predict the loads on a wing were those of Prandtl¹⁵. Prandtl's lifting line theory modeled large aspect ratio wings using a single bound vortex line. Later, Pistoletti¹⁶ proposed the 1/4 - 3/4 chord concept, finding

that, with the vortex at the $1/4 c$ and the downwash point at the $3/4 c$, accurate predictions could be made for the section lift and moment coefficients. Falkner¹⁷ was the first to use the name vortex lattice theory but the development of the method had to await computer capability. The mid-sixties saw the beginning of the computational vortex lattice method (VLM). For further reviews of the development of the vortex lattice method, the reader is referred to DeYoung¹⁸ and Parker¹⁹.

Belotserkovskiy²⁰ developed the first successful nonlinear steady numerical method to calculate the loads on a wing with tip separation. The wing was replaced by a bound vortex lattice and the wake by vortex filaments. Later, Belotserkovskiy and Nisht²¹ developed a method for highly swept wings in unsteady flow with tip separation.

Using a method similar to that of Belotserkovskiy, Maddox²² added leading edge separation to the basic VLM. The leading edge wake was represented by discrete vortex lines which were allowed to move with the flow field to achieve a force free wake. Kandil²³ extended the approach to include a force free trailing edge wake. Agreement with experimental results was very good. Extending the VLM to treat unsteady flows, Atta²⁴ looked at rectangular wings with separation along the sharp edges. Thrasher et al.²⁵ and Thrasher²⁶ reposed the problem using a body fixed reference frame and were able to treat the unsteady flow over a low aspect ratio wing executing an arbitrary maneuver. The method was further refined by Atta²⁷ and Konstadinopoulos²⁸. The present method is based on the work of Konstadinopoulos. The method is completely general as long as separation takes place only along sharp edges and vortex bursting does not occur.

Chapter Three

STATEMENT OF PROBLEM AND METHOD OF SOLUTION

3.1 Problem Statement

The flow of an incompressible, inviscid fluid over a delta wing with and without leading edge flaps is to be modeled. Using a general vortex lattice method with the assumptions that separation occurs only along sharp edges and vortex bursting does not occur, the pressure distributions and aerodynamic loads are found.

3.2 The Basic Method

The flow, steady or unsteady, of an incompressible, inviscid fluid about a thin, finite wing can be modeled by representing the wing with a bound vortex sheet and the wakes, both leading and trailing edge, with free vortex sheets. Across the bound vortex sheet, a pressure jump exists while across the free vortex sheet there is no pressure difference and the sheet is allowed to deform to a force-free position. The vortex sheets are replaced by a lattice of short, straight vortex segments. The velocity generated by the discrete vortex lines can be calculated using the Biot-Savart law. Referring to Figure 4, the velocity due to the vortex segment at any point P is given by

$$\vec{V}_p = \frac{\Gamma}{4\pi h} (\cos\theta_1 - \cos\theta_2) \vec{e}_v$$

where $\vec{e}_v = \vec{e}_w \times \vec{r}_1 / |\vec{r}_1|$

and $h = |\vec{r}_1 \times \vec{e}_w|$

The governing equation for the velocity field is the continuity equation. For an incompressible fluid,

$$\vec{\nabla} \cdot \vec{V} = 0$$

Since the velocity is found using the Biot-Savart law, this equation is automatically satisfied. For a general unsteady flow, the accompanying boundary conditions are as follows:

- (1) The fluid cannot penetrate the lifting surface.

Thus,
$$(\vec{V} - \vec{V}_{LS}) \cdot \vec{n} = 0 \quad \text{on } S_{LS}$$

where \vec{V} is the absolute velocity of a fluid particle, \vec{V}_{LS} is the velocity of the lifting surface, \vec{n} is the unit normal, and S_{LS} is the lifting surface. In the VLM, this condition is satisfied only at the control points.

- (2) All disturbances created by the lifting surface must die out away from the surface and its wake.

That is,
$$|\vec{V}| \rightarrow 0 \quad \text{away from } S_{LS} \text{ and } S_W$$

where S_W is the wake surface. Again, this is automatically satisfied by using the Biot-Savart law to calculate the velocities.

- (3) There cannot be any discontinuity in the pressure in the wake. A force free wake is obtained by applying the Kelvin-Helmholtz theorem on the wake.

$$\frac{D\Gamma}{Dt} = 0 \quad \text{on } S_W$$

where Γ is the circulation around any closed loop.

- (4) There must be spatial conservation of circulation. That is, the net flux of vorticity through any closed surface is zero everywhere

in the flow. Hence,

$$\operatorname{div} \vec{\xi} = \operatorname{div}(\operatorname{curl} V) = 0$$

where $\vec{\xi}$ is the vorticity.

(5) The Kutta condition for unsteady flow is enforced. There are various interpretations of the Kutta condition as applied to the VLM. Among them are the following

- a) the velocity at the trailing edge must be finite
- b) the rear stagnation point must be at the trailing edge
- c) the velocities on the upper and lower surfaces at the trailing edge must allow the flow to separate smoothly
- d) the velocity potential at the trailing edge must be continuous
- e) C_p must be zero at the trailing edge.

For steady flow, the above all yield the same results, but for unsteady flow, different Kutta conditions can yield different results. The Kutta condition incorporates the effects of viscosity into the flow but the particular interpretation which should be used depends on the mathematical model. The present model applies the Kutta condition by insuring that the flow is tangent along the sharp edges where separation occurs.

In this unsteady model as conditions change with time starting vortices form along the sharp edges. These are then shed and convected downstream with the local particle velocity. Hence the wake is represented by a lattice rather than a set of discrete vortex lines as in the steady model. When conditions stop changing, i.e., for steady

flow, vorticity continues to be shed but the strengths tend to become constant until a steady state is achieved. Figure 5 shows the formation of the leading and trailing edge wakes, spread out for clarity.

3.3 Lattice Arrangement

Following the usual VLM practice, the wing is divided into panels, each of which is made up of vortex segments. The vortex lattice as a whole is offset from the actual wing by $1/4$ of the panel chord, as depicted in Figure 6. Control points, where the no-flow condition is applied, are placed at the centroids of the vortex elements. In the present method, control points were placed on only half of the wing using symmetric properties to account for effects from the other half of the wing. Thus, only symmetric configurations could be considered but computer time was reduced by almost one-half. The overall distribution of the elements is chordwise uniform. Hough²⁹ noted that cosine spacing of the control points does not improve convergence for wings with flaps. To insure rapid convergence, he recommended the placement of bound vortices along the hingeline. Although convergence was achieved in the present work without this arrangement, the recommendation is noted here as a means of future improvement.

The preferred element shape is rectangular for the most accurate results as shown by Kelly³⁰. However, the shape must be changed along the leading edge of a delta wing. For the plain wing, trapezoidal elements are used and for the flapped wing, pentagonal elements are used. The vortex segments along the leading edge are normal to the edge which has been found by Kandil²³ and Kelly³⁰ to give best results.

The leading edge flap was deflected at 30° which has been found^{11,12} to be the optimum setting. The flap area was approximately 26 percent of the wing area, with a flap chord 6.7 percent of the wing mean aerodynamic chord.

3.4 Method of Solution

The method of solution is a time stepped procedure. First the lattice is set up and the influence coefficients are calculated for each control point using the Biot-Savart law. The circulations around each vortex element are then determined by applying the no-flow condition and the spatial conservation of circulation condition. While the circulations are held constant, the wake position is found for a force free wake by aligning the upstream end of each segment with the local particle velocity. The last two steps are repeated until the wake shape becomes constant.

3.5 Calculation of Loads

To determine the loads on the wing, the force on each element in the bound lattice is found by calculating the pressure jump at the control point and multiplying by the area of the element. The pressure coefficients are found using the unsteady Bernoulli equation as follows,

$$\frac{\partial \phi^*}{\partial t^*} + \frac{V^{*2}}{2} + \frac{p^*}{\rho} = F(t)$$

where the star denotes physical quantities, ϕ^* is the absolute velocity potential in the inertial frame, V^* is the velocity relative to the inertial frame, and $F(t)$ is a function of time. Converting to

dimensionless quantities yields,

$$\frac{\partial \phi}{\partial t} + \frac{V^2}{2} + \frac{P^*}{\rho U^2} = \frac{F(t)}{U^2}$$

Since the boundary condition for the velocity at infinity is $|V| \rightarrow 0$ and $\phi(\infty)$ is a constant, the above equation at infinity becomes,

$$\frac{P_{\infty}^*}{\rho U^2} = \frac{F(t)}{U^2}$$

Thus the non-dimensional pressure coefficient is,

$$C_p = \frac{P^* - P_{\infty}^*}{\frac{1}{2} \rho U^2} = -2 \frac{\partial \phi}{\partial t} - V^2$$

In the present model, the problem is posed in a wing fixed reference frame rather than a ground fixed or inertial frame. Refer to Figure 7a. Hence the above equation, in which the time derivative is taken with respect to an inertial frame, must be transformed to the moving, wing fixed system. Using,

$$\frac{\partial \phi}{\partial t} = \frac{\partial \phi}{\partial t} - \vec{\nabla} \phi \cdot (\vec{V}_A + \vec{\Omega} \times \vec{r})$$

where ϕ is the velocity potential in the moving frame, \vec{V}_A is the velocity of the origin of the moving frame with respect to the inertial frame, $\vec{\Omega}$ is the angular velocity of the moving frame, and \vec{r} is the position vector in the moving frame. Thus,

$$C_p = -2 \frac{\partial \phi}{\partial t} - \vec{V} \cdot (\vec{V} - 2\vec{V}_A - 2\vec{\Omega} \times \vec{r})$$

where \vec{V} is the velocity of a particle relative to the inertial frame.

The pressure difference between the upper and lower surfaces is

$$\Delta C_p = C_{p_u} - C_{p_l} = -2 \left(\frac{\partial \phi_u}{\partial t} - \frac{\partial \phi_l}{\partial t} \right) + 2(\vec{V}_u - \vec{V}_l) \cdot (\vec{V}_A + \vec{\Omega} \times \vec{r}) - (\vec{V}_u - \vec{V}_l) \cdot (\vec{V}_u + \vec{V}_l)$$

The individual terms are calculated as follows. First using

$$\begin{aligned} \vec{V}_u &= \vec{V}_m + \Delta\vec{V} \\ \vec{V}_l &= \vec{V}_m - \Delta\vec{V} \end{aligned}$$

where \vec{V}_m is the velocity generated at the control point by all the vortex segments except those around the element and $\Delta\vec{V}$ is the velocity jump across the vortex sheet. To evaluate the unsteady term, the quantity $\phi_u - \phi_l$ is first found using,

$$\phi_u - \phi_l = \int_C \vec{\nabla}\phi \cdot d\mathbf{S}$$

Since $\vec{\nabla}\phi$ is tangent to the wing at the control point, the circuit of integration can be closed to give,

$$\phi_u - \phi_l = \oint_C \vec{\nabla}\phi \cdot d\mathbf{S} = G_i$$

where G_i is the circulation around the i^{th} element. See Figure 7.

The time derivative can then be approximated as follows,

$$\frac{\partial}{\partial t} (\phi_u - \phi_l) \approx \frac{G_i(t + \Delta t) - G_i(t)}{\Delta t}$$

where $G_i(t)$ and $G_i(t + \Delta t)$ are the stored values of G_i at successive time intervals. The velocity jump $\Delta\vec{V}$ is

$$\Delta\vec{V} = \vec{V}_u - \vec{V}_l = \vec{\xi} \times \vec{n}$$

where $\vec{\xi}$ is the vorticity per unit area and \vec{n} is the normal to the

surface. To evaluate $\vec{\xi}$, an average vorticity is defined,

$$\vec{\xi} \approx \vec{\xi}_{\text{ave}} = \sum_k \frac{F \Gamma_k \vec{l}_k}{2A}$$

where the sum is taken around the element, Γ_k is the individual segment circulation (see Figure 7b), \vec{l}_k is the position vector along the segment, A is the area of the element, and F is a constant with value 1 for interior elements and 2 for the first row elements. Along the leading edge, the contributions from segments that are not normal or tangential to the edge are omitted to allow the equation to reduce to the proper form for steady flow (where all vorticity leaves the wing normal to the edge).

The last term is easily evaluated using

$$V_u + V_l = 2V_m .$$

Once the pressure differences at each element are known, they can be summed over the entire surface to give the aerodynamic loads. The normal force coefficient is found using

$$C_N = \frac{- \sum_i (\Delta C_{p_i} a_i + \Delta C_{pf_i} a_{f_i} \cos \delta)}{A_t}$$

where a_i is the area of the panel element, f denotes flap quantities, δ is the flap deflection angle, A_t is the total area of the wing plus the projected flap area, such that

$$A_t = \sum (a_i + a_{f_i} \cos \delta)$$

An axial force exists whenever the flap is deflected and is found using

$$C_A = \frac{\sum \Delta C_{pfi} a_{fi} \sin \delta \sin(\text{csweep})}{A_t}$$

where csweep is the complimentary sweep angle.

Lift and drag coefficients are found using,

$$C_L = C_N \cos \alpha - C_A \sin \alpha$$

$$C_D = C_N \sin \alpha + C_A \cos \alpha$$

Pitching moment is calculated by multiplying the distance from the leading edge to the control point of the element times the force on the element and summing over the entire surface. It is then converted to the moment about the quarter mean aerodynamic chord which is at the half chord for a delta wing.

3.6 Notes on Convergence and Computer Times

There are two conditions for convergence. First, for any given number of elements the time stepped procedure must converge, i.e., for steady flow the wake must become steady and the unsteady terms must go to zero. Second, as the number of elements is increased, the aerodynamic loads must converge to a constant value.

To minimize computation time the program was run using the minimum number of panels required for convergence. For the plain half wing 10 control points were used while for the flapped half wing 15 control points were necessary. The average number of time steps required for convergence was 20 for the plain wing and 30 for the flapped wing. At 5° angle of attack convergence for the flapped wing was poor. Table 1 gives sample computer times on an IBM 370/158.

Chapter Four

NUMERICAL RESULTS

The present method was applied to a 75° flat delta with and without constant chord leading edge flaps. The plain wing was run at angles of attack ranging from 5° to 35° . The upper limit was chosen because experimental results, Marchman¹² and Wentz¹⁰, show that stall occurs at approximately 36° . A lattice of 4 chordwise rows was used, giving pressures at 10 locations on the half wing. Figures 8, 9, and 10 show the pressure difference coefficient at angles of attack of 10, 20, and 30° respectively. For comparison, the experimental data of Wentz is shown. Wentz' model was a 74° flat delta. At 20° angle of attack, another method, the Free Vortex Sheet (FVS), Johnson *et al.*⁵, is also shown. Comparison with both experimental results and the FVS method is very good at 10° . At 20° , comparison is good except at the trailing edge row where the present method shows a slight shift in the position of the vortex towards the centerline of the wing. This is probably due to the coarse lattice used. At 30° the present method does not predict the strong vortex peaks shown in the experimental data, except at the apex row where agreement is good.

The wing with flaps was run at angles of attack from 5° to 20° . Here, five chordwise rows were used giving pressures at 10 stations on the half wing and 5 on the flap. Because of the lack of pressure data for a leading edge flapped wing, results are compared with Wentz' data¹⁰ for a conical camber and an apex cambered wing. Referring to

Figure 11, at 10° the leading edge flap gives very similar results to the conical camber model, although at the trailing edge of the wing the pressure difference coefficient for the leading edge flap is closer to the apex camber data as might be expected. At 20° , shown in Figure 12, agreement is similar except at the apex where the apex camber shows very little lift and the leading edge flap predicts a strong vortex lift. Figure 13 shows the vortex flap at 10 , 15 , and 20° . Comparisons of the plain wing and the wing with flap show that indeed the leading vortex flap does keep the vortex flow along the leading edge. Figures 14 and 15 show the wakes of the plain wing and the flapped wing, respectively, at 15° angle of attack.

Results for lift coefficient versus angle of attack are shown in Figures 16 through 18. Comparison of the plain wing, Figure 16, is made using experimental data of Marchman¹², Wentz¹⁰, Peckham⁹ and theory of Polhamus¹⁴. The present method shows agreement well within the range of experimental data. At the higher angles of attack, both the present model and theory of Polhamus begin to deviate from experimental results due to the approach of vortex bursting and stall. Results of lift coefficient for the leading edge flap are shown in Figure 17. Also presented are the experimental results of Marchman's 75° delta with 30° flap¹² and Wentz' 74° delta with 24° flap¹⁰. Again agreement is good except at 20° where the present method predicts too high a value for the lift coefficient. Figure 18 shows both the plain delta and the leading edge flap delta along with the experimental results of Marchman¹² and Wentz¹⁰. The present method shows the same general conclusion that the experimental results show, the addition of a

leading edge flap does not substantially change the lift coefficient except at the higher angles of attack. Here the results show that at 20° , the leading edge flap begins to show an increase in the lift coefficient while results of Marchman¹² show an increase occurring at approximately 25° .

The effect of the leading edge flap is seen more clearly in the results of axial force. Figure 19 shows the axial force of the present method along with experimental data as a function of $\sin^2\alpha$, since both the edge force and the vortex flow terms have this dependency. Agreement is especially good at the higher angles of attack. Because axial force is sensitive to the edge flow, it can be used to determine when flow changes occur on the wing. The change in the curve at 10° , where $\sin^2\alpha = 0.03$, suggests a flow change. At angles less than 10° the leading edge vortex is trying to form on the lower surface of the flap which is not allowed in the present code, while above 10° , the leading edge vortex is positioned on the upper surface.

Results for the drag polar are shown in Figure 20. At 5° or above, the leading edge flap shows a reduction in drag coefficient over the plain wing. Calculated drag coefficients for both the plain and flapped wing are slightly lower than for experimental results, as can be expected due to lack of skin friction in the present model. However, the reductions in drag are comparable, approximately 23 percent at C_L of 0.85.

Pitching moment coefficient versus angle of attack is presented in Figure 21. The plain wing results are good up to 20° where a jump occurs in the values. This is probably due to a shift in the center

of pressure at angles of 25° and higher. At these high angles, the present method does not accurately locate the vortex core as seen in Figure 10. The leading edge flap shows the general trend of increasing the pitching moment at low angles of attack but improving at higher angles. Agreement with Rao's¹¹ data is good at higher angles.

Chapter Five

CONCLUSIONS AND RECOMMENDATIONS

Using a general unsteady nonlinear vortex lattice method, the aerodynamic loads have been found for a 75° delta wing with and without leading edge vortex flaps. Limited computer funds prevented finer lattice computations. Even so, the coarse lattice was able to predict pressures and forces that compared well with experimental data from several sources. The results show that the vortex flap can substantially reduce drag and even increase lift at higher angles of attack. At lower angles of attack, the constant chord flap model shows a destabilizing trend in the pitching moment but at higher angles of attack, the pitching moment slope of the flapped wing becomes equal to that of the plain wing.

Limitations in the method occur at very low (5° and below) and high (above 20°) angles of attack where convergence becomes slow. This problem with convergence has been noted in other methods^{4,31}.

Further work needs to be done on the best placement of a minimum number of control points for the most accurate results. The placement of a bound vortex along the hingeline should also improve accuracy. Other suggestions for future study include the investigation of asymmetric flows, different flap shapes, and the use of more realistic wing configurations.

REFERENCES

1. Campbell, J. F., "Augmentation of Vortex Lift by Spanwise Blowing," *Journal of Aircraft*, Vol. 13, No. 9, Sept. 1976, pp. 727-732.
2. Purvis, J. W., "Analytical Prediction of Vortex Lift," *Journal of Aircraft*, Vol. 18, No. 4, April 1981, pp. 225-230.
3. Kuhlman, J., "Load Distributions on Slender Delta Wings Having Vortex Flow," *Journal of Aircraft*, Vol. 14, No. 7, July 1977, pp. 699-702.
4. Reddy, C. S., "Investigation of Aerodynamic Characteristics of Wings Having Vortex Flow Using Different Numerical Codes," NASA CR-165706, April 1981.
5. Johnson, F. T., Lu, P., Tinoco, E. N. and Epton, M. A., "An Improved Panel Method for the Solution of 3-D Leading Edge Vortex Flows. Volume 1 Theory Document," NASA CR-3278, July 1980.
6. Winter, H., "Flow Phenomena on Plates and Airfoils of Short Span," NACA TM 798, 1937.
7. Whittle, E. F. Jr., and Lovell, J. C., "Full Scale Investigation of an Equilateral Triangular Wing Having 10-Percent-Thick Biconvex Airfoil Sections," NACA RM L8G05, Sept. 1948.
8. Bartlett, G. E. and Vidal, R. J., "Experimental Investigation of Influence of Edge Shape on the Aerodynamic Characteristics of Low-Aspect-Ratio Wings at Low Speeds," *Journal of Aeronautical Sciences*, Vol. 22, No. 8, August 1955, pp. 517-533.
9. Peckham, D. H., "Low-Speed Wind-Tunnel Tests on a Series of Uncambered Slender Pointed Wings with Sharp Edges," R & M No. 3186, British ARC, 1961.
10. Wentz, W. H. Jr., "Effects of Leading-Edge Camber on Low-Speed Characteristics of Slender Delta Wings," NASA CR-2002, October 1972.
11. Rao, D. M., "Leading Edge Vortex-Flap Experiments on a 74° Delta Wing," NASA CR 159161, Nov. 1979.
12. Marchman, J. F. III, "Effectiveness of Leading-Edge Vortex Flaps on 60 and 75 Degree Delta Wings," *Journal of Aircraft*, Vol. 18, No. 4, April 1981, pp. 280-286.

13. Polhamus, E. C., "A Concept of the Vortex Lift of Sharp-Edge Delta Wings Based on a Leading-Edge-Suction Analogy," NASA TN D-3767, Dec. 1966.
14. Polhamus, E. C., "Predictions of Vortex-Lift Characteristics by a Leading-Edge Suction Analogy," Journal of Aircraft, Vol. 8, No. 4, April 1971.
15. Karamcheti, K., Principles of Ideal-Fluid Aerodynamics, Krieger Publishing Co., Huntington, New York, 1980.
16. Pistolesi, E., "Considerations on the Mutual Interference of Airfoil Systems," L.G.L. Report, 1937, pp. 214-219.
17. Falkner, V. M., "The Accuracy of Calculations Based on Vortex Lattice Theory," Rep. No. 9621, British ARC, 1946.
18. DeYoung, J., "Historical Evolution of Vortex Lattice Methods," NASA SP-405, May 1976.
19. Parker, A. G., "Aerodynamic Characteristics of Slender Wings with Sharp Leading Edges--A Review," Journal of Aircraft, Vol. 13, March 1976, pp. 161-168.
20. Belotserkovskiy, S. M., "Calculation of the Flow Around Wings of Arbitrary Planforms in a Wide Range of Angles of Attack," NASA TT F-12, 291, 1969.
21. Belotserkovskiy, S. M. and Nisht, M. I., "Nonstationary Nonlinear Theory of a Thin Wing of Arbitrary Planform," Fluid Dynamics, Vol. 9, No. 4, 1974, pp. 583-589.
22. Maddox, S. A., "An Extension of a Vortex-Lattice Method to Include the Effects of Leading-Edge Separation," M.S. Thesis, Dept. Engineering Science and Mechanics, Virginia Polytechnic Institute and State University, Blacksburg, Virginia, July 1973.
23. Kandil, O. A., "Prediction of the Steady Aerodynamic Loads on Lifting Surfaces Having Sharp-Edge Separation," Ph.D. Dissertation, Engineering Science and Mechanics Dept., Virginia Polytechnic Institute and State University, December 1974.
24. Atta, E. H., "Unsteady Flow over Arbitrary Wing-Planforms Including Tip Separation," M.S. Thesis, Dept. of Engineering Science and Mechanics, Virginia Polytechnic Institute and State University, Blacksburg, Virginia, March 1976.
25. Thrasher, D. F., Mook, D. T., Kandil, O., and Nayfeh, A. H., "Application of the Vortex-Lattice Concept to General, Unsteady Lifting-Surface Problems," AIAA Paper No. 77-1157, 1977.

26. Thrasher, D. F., "Nonlinear Unsteady Aerodynamics with Application to Dynamic-Aerodynamic Interaction," M.S. Thesis, Dept. of Engineering Science and Mechanics, Virginia Polytechnic Institute and State University, Blacksburg, Virginia, May 1979.
27. Atta, E. H., "Nonlinear Steady and Unsteady Aerodynamics of Wings and Wing-Body Combinations," Ph.D. Dissertation, Dept. of Engineering Science and Mechanics, Virginia Polytechnic Institute and State University, Blacksburg, Virginia, May 1978.
28. Konstadinopoulos, P., Mook, D. T., and Nayfeh, A. H., "A Numerical Method for General, Unsteady Aerodynamics," AIAA-81-1877, August 1981.
29. Hough, G. R., "Lattice Arrangements for Rapid Convergence," NASA SP-405, May 1976.
30. Kelly, S. G., "A Systematic Investigation of the Parameters Affecting the Accuracy of the Vortex-Lattice Method," M.S. Thesis, Dept. of Engineering Science and Mechanics, Virginia Polytechnic Institute and State University, Blacksburg, Virginia, May 1977.
31. Kuhlman, J. M., "Analytical Studies of Separated Vortex Flow on Highly Swept Wings," NASA CR-3022, Nov. 1978.

Table 1. Calculation times for various configurations

CPU Times on an IBM 370/158

	Full Wing	
	No. of time steps	CPU time (min.)
4 rows (20 control points) no flap	20	3.49
	25	4.40
	Half Wing	
	No. of time steps	CPU time (min.)
4 rows (10 control points) no flap	20	2.04
	30	3.81
5 rows (15 control points) 30° flap	30	6.48
6 rows (21 control points) 30° flap	30	13.30

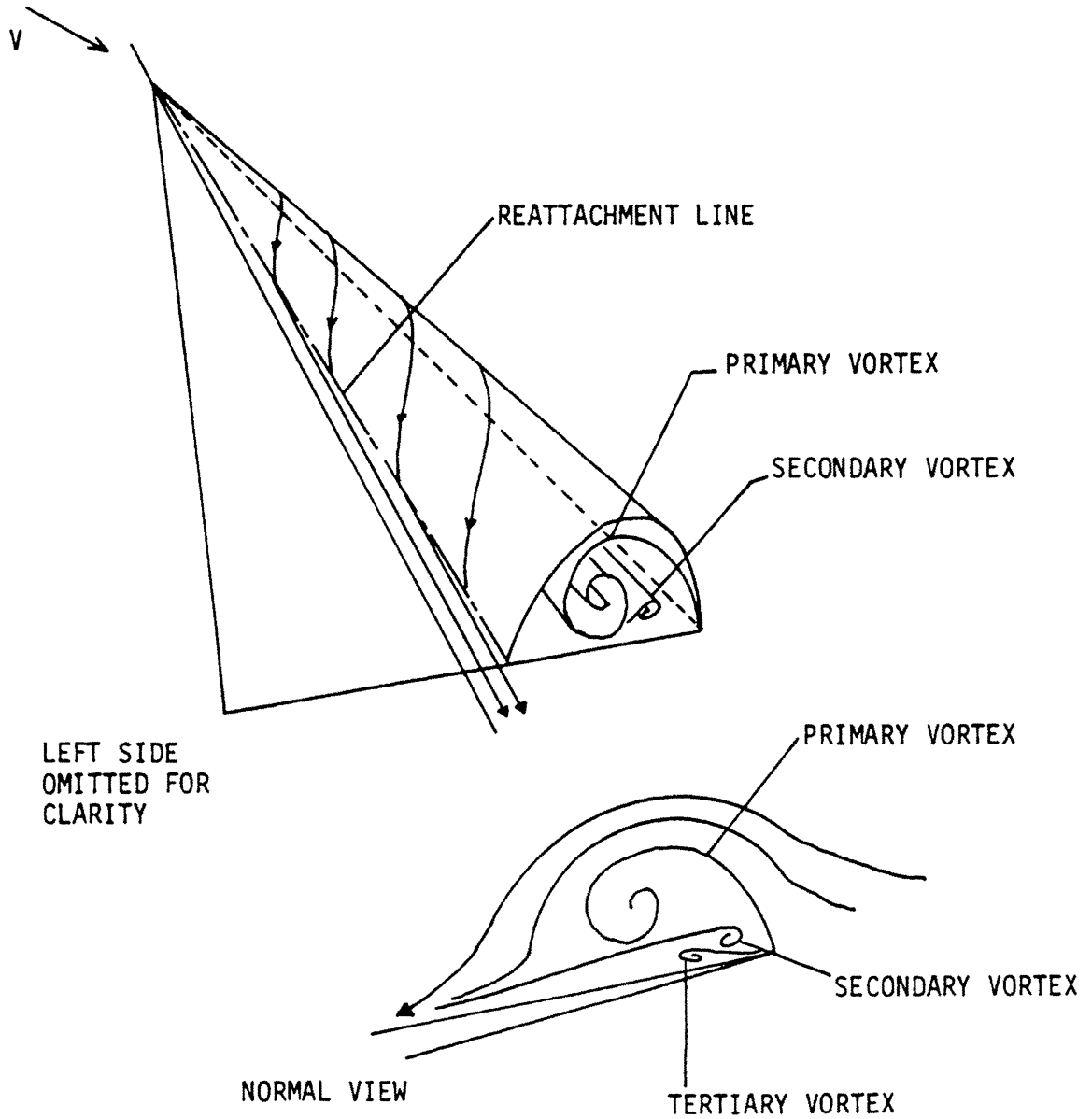


Figure 1. Flow field over a delta wing
with leading edge separation

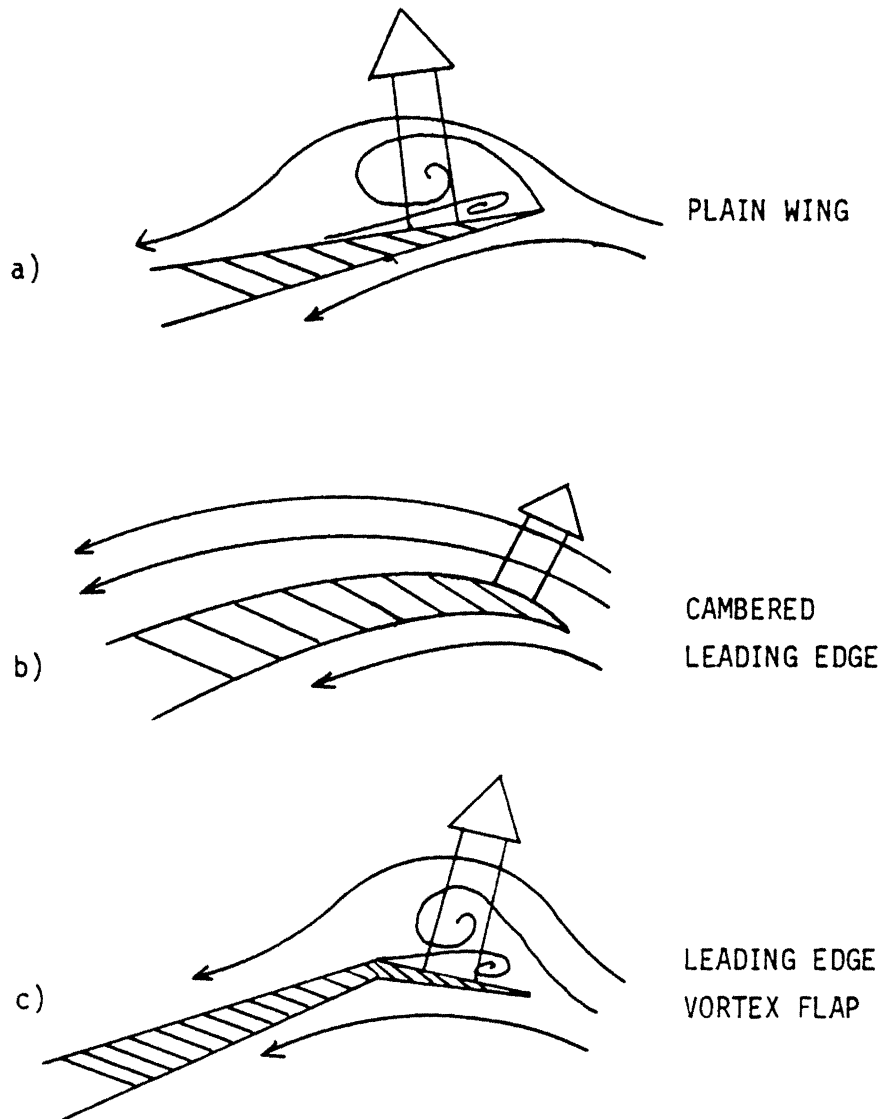


Figure 2. Resultant force on various leading edges

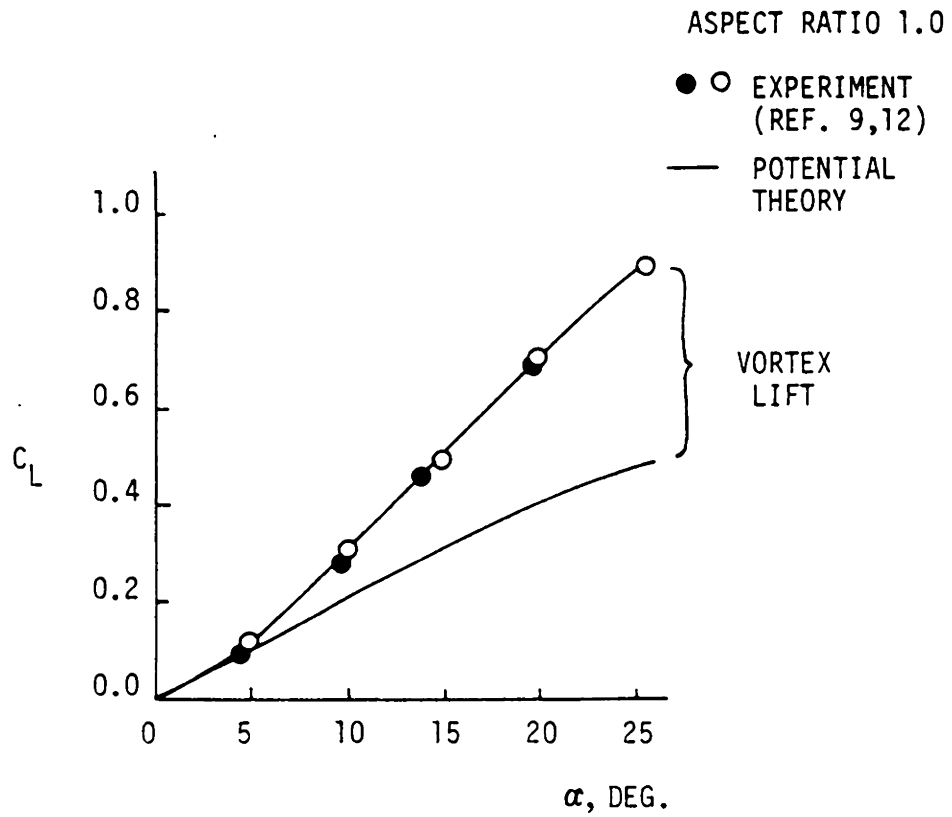


Figure 3. Nonlinear aspect of aerodynamic loads on wings with vortex lift

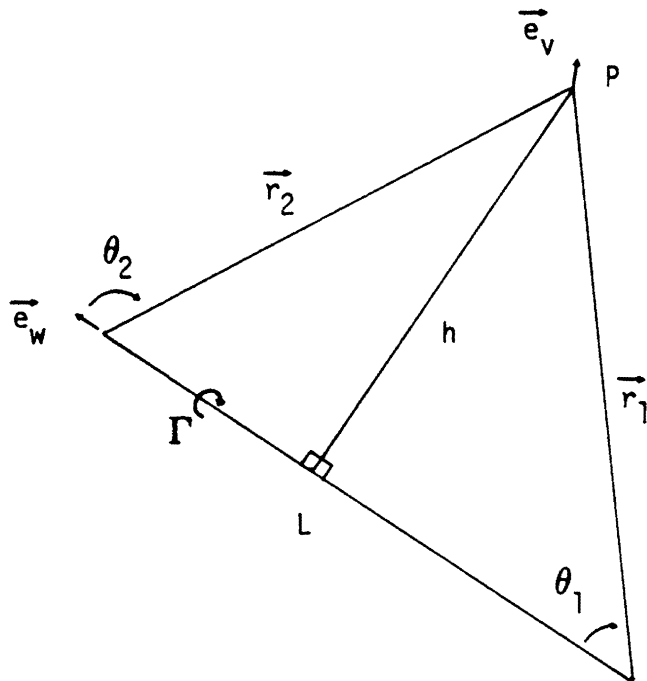


Figure 4. Biot-Savart law

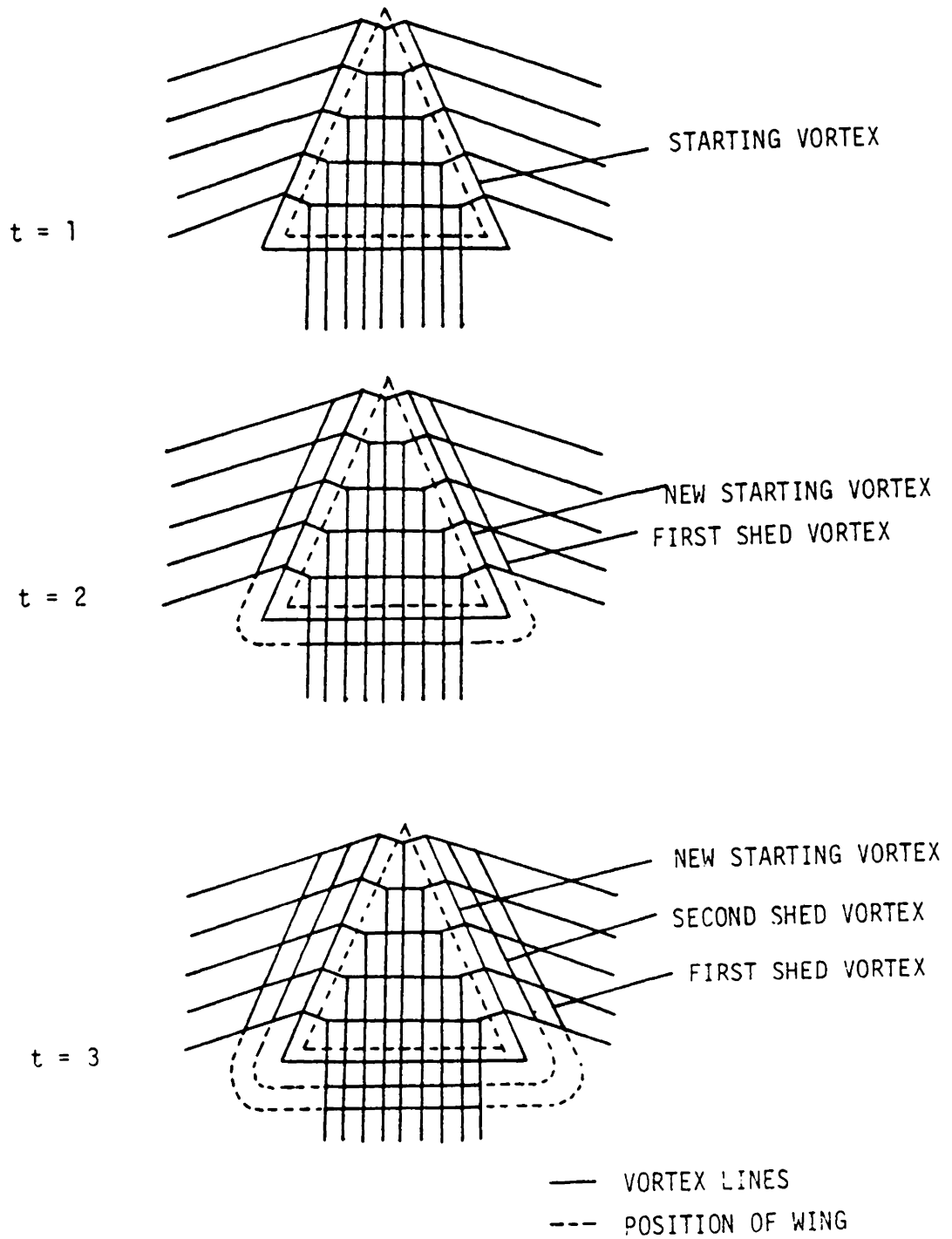


Figure 5. Shed vortex lines

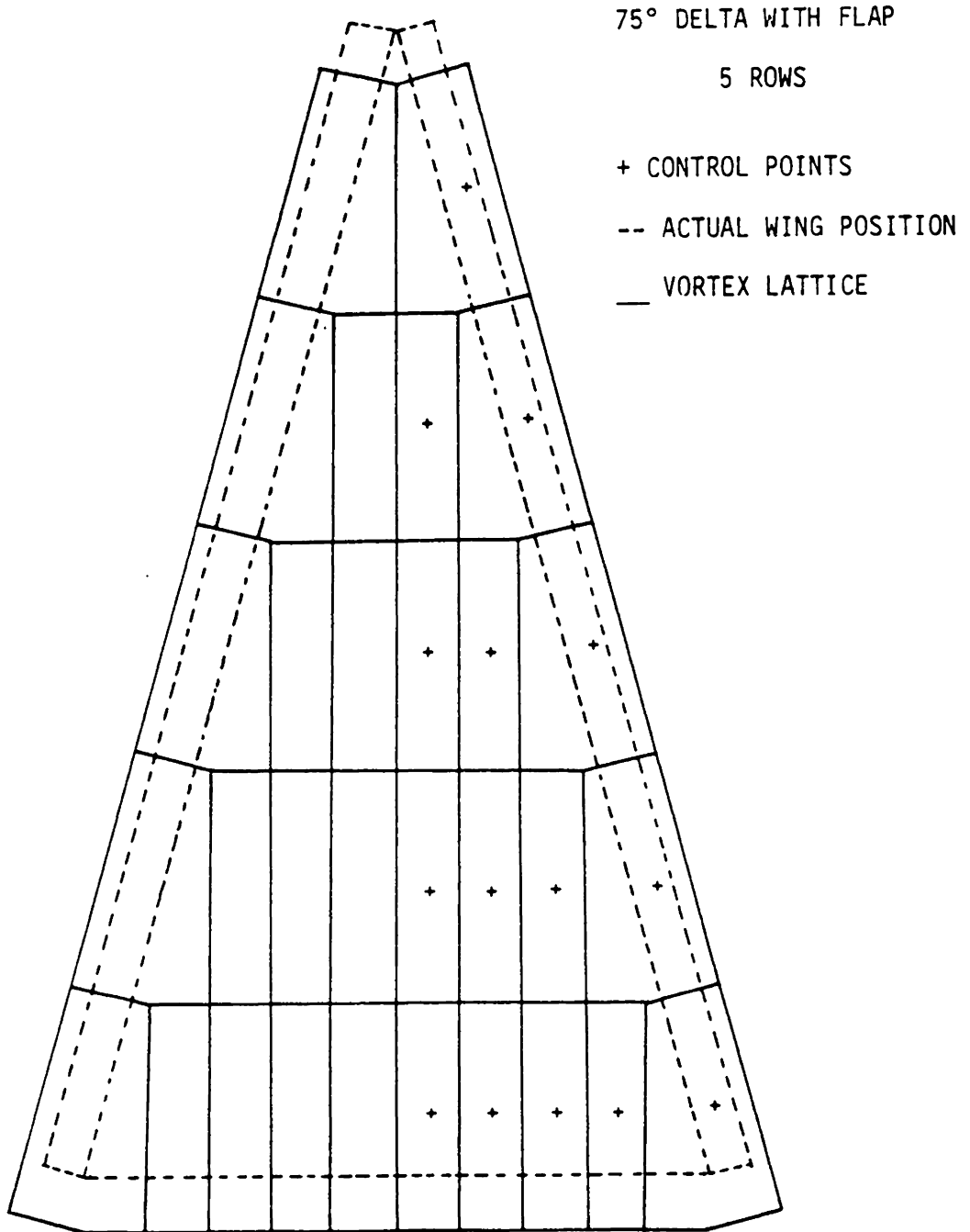
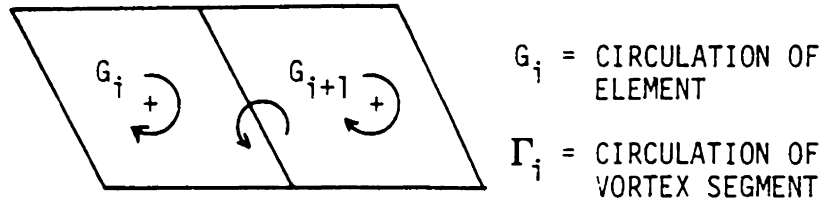
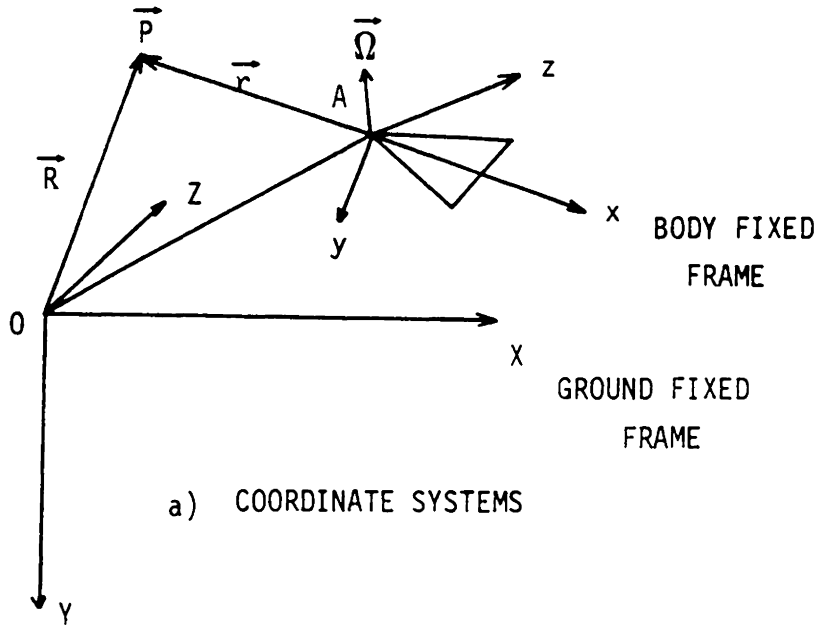


Figure 6. Vortex lattice



$$\Gamma_i = G_i - G_{i+1}$$

b) DEFINITION OF CIRCULATIONS

Figure 7. Definitions for calculations of loads using Bernoulli's equation

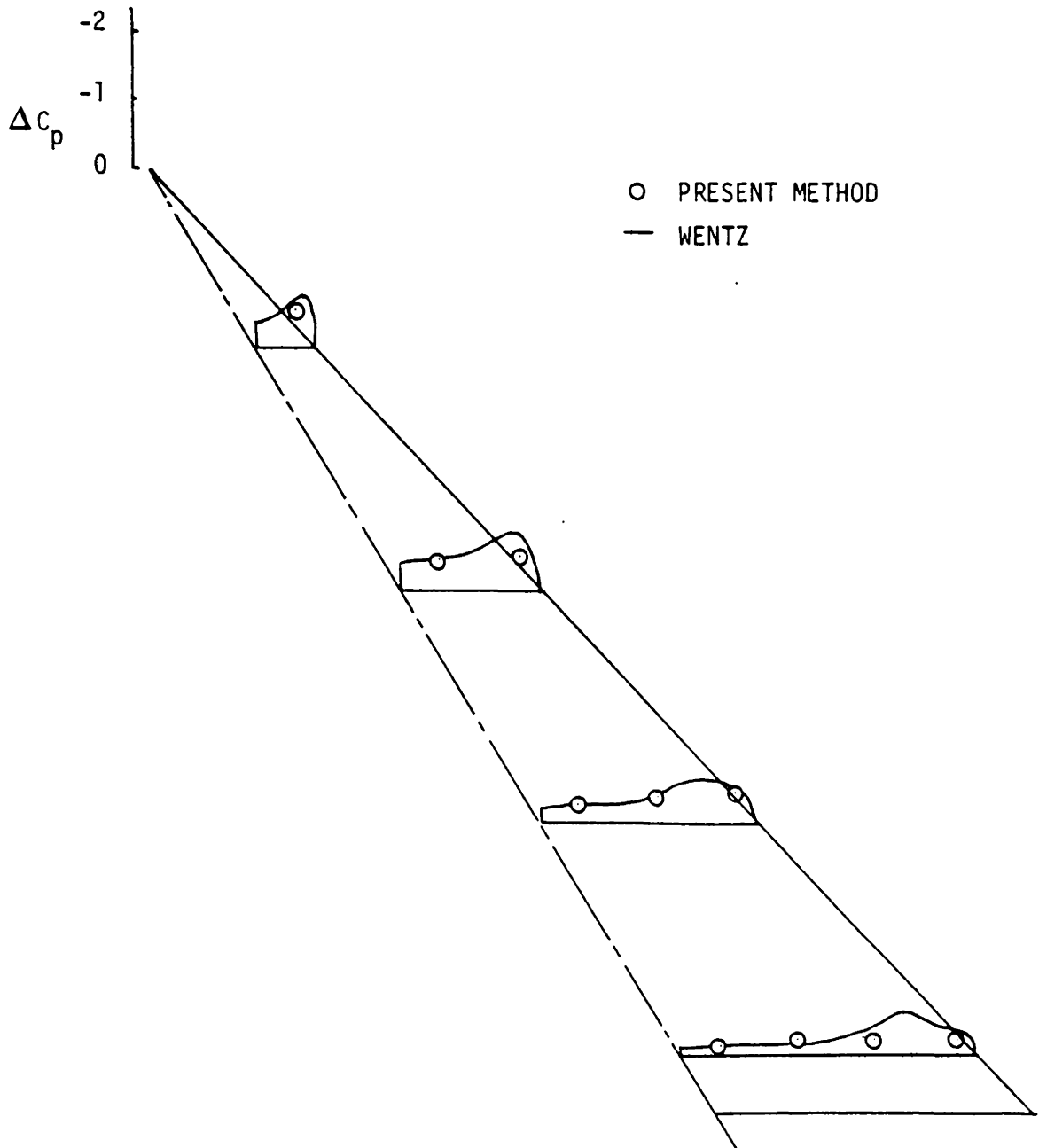


Figure 8. Pressure distribution - flat delta
 $\alpha = 10^\circ$

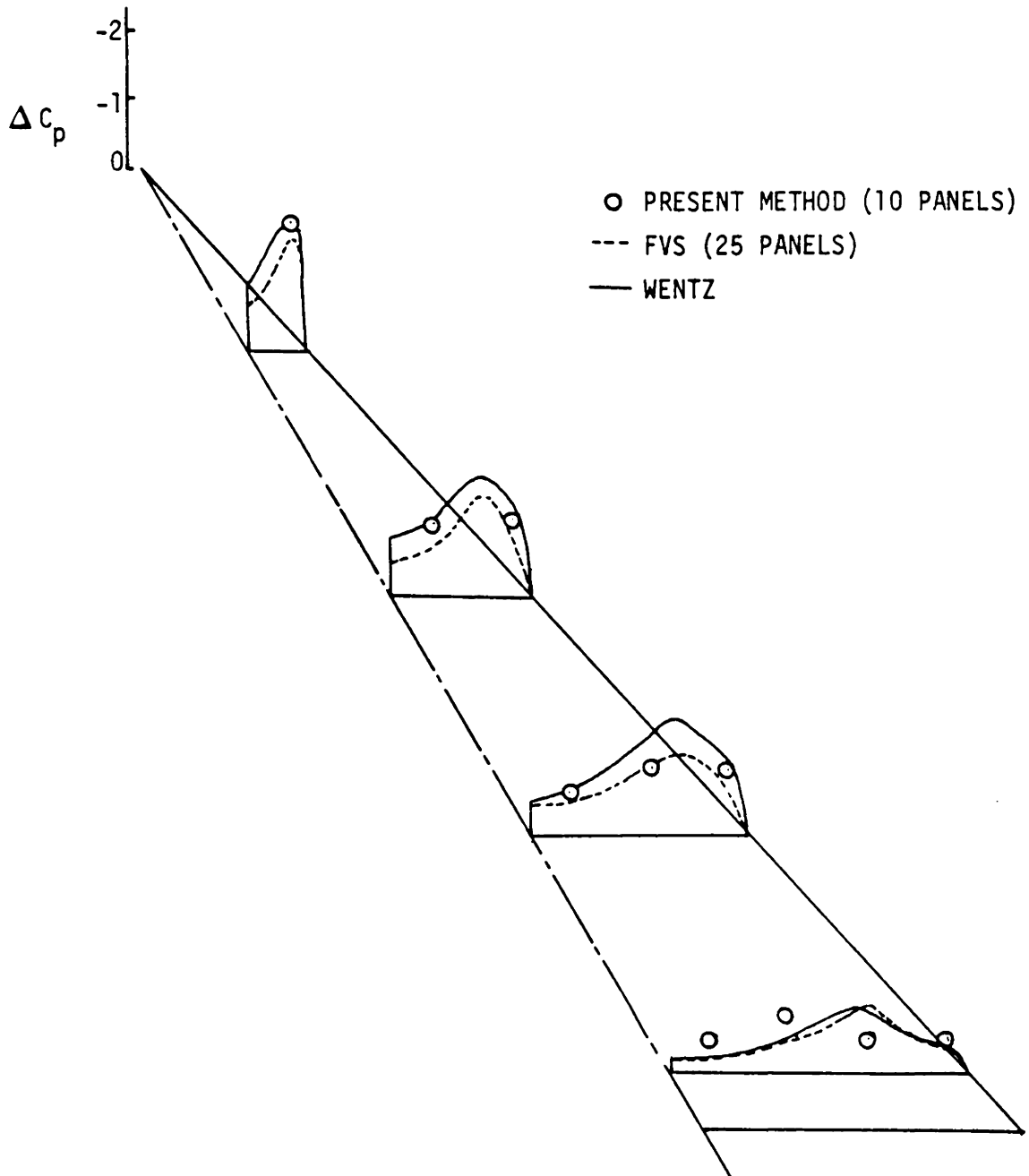


Figure 9. Pressure distribution - flat delta
 $\alpha = 20^\circ$

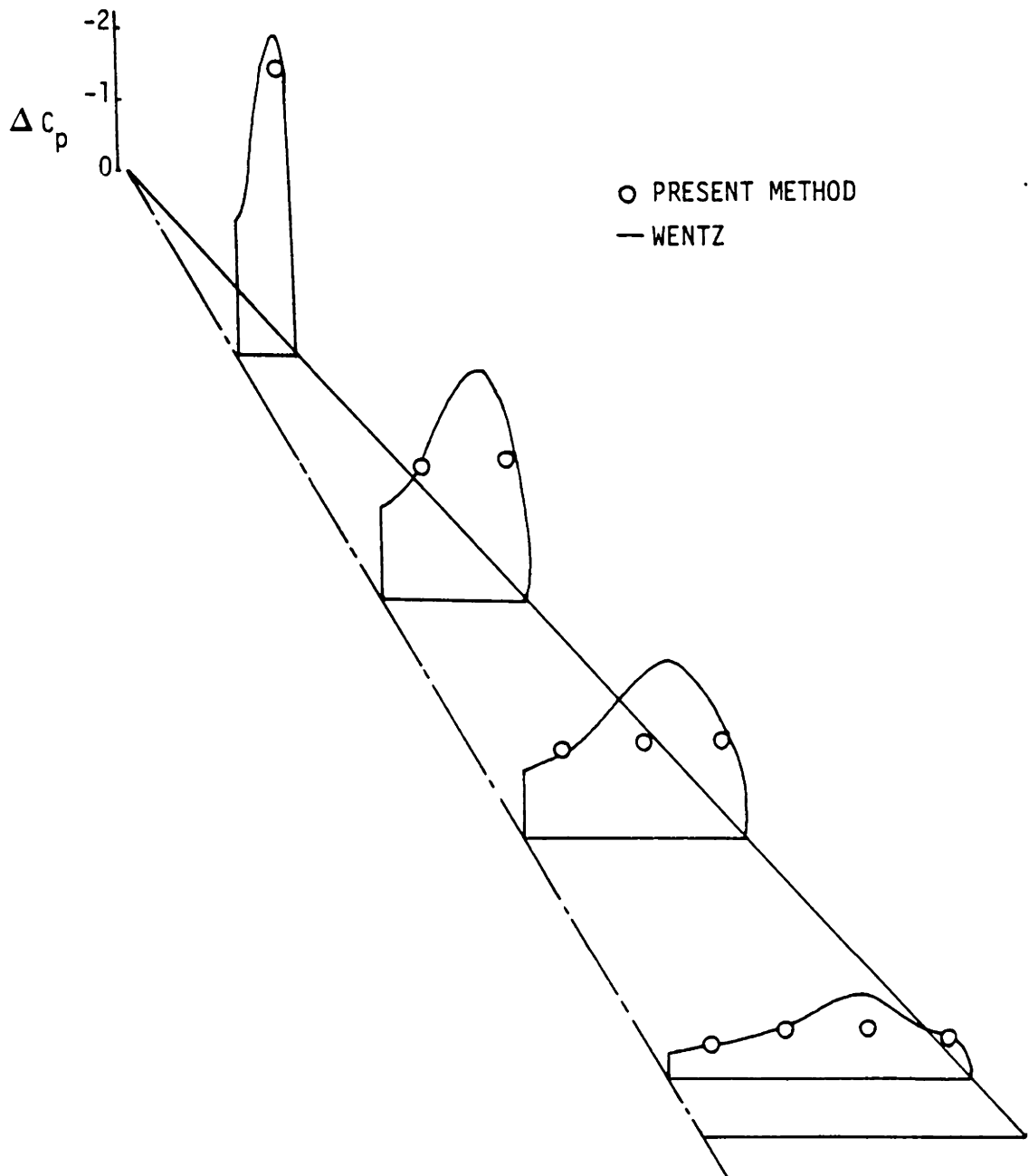


Figure 10. Pressure distribution - flat delta

$$\alpha = 30^\circ$$

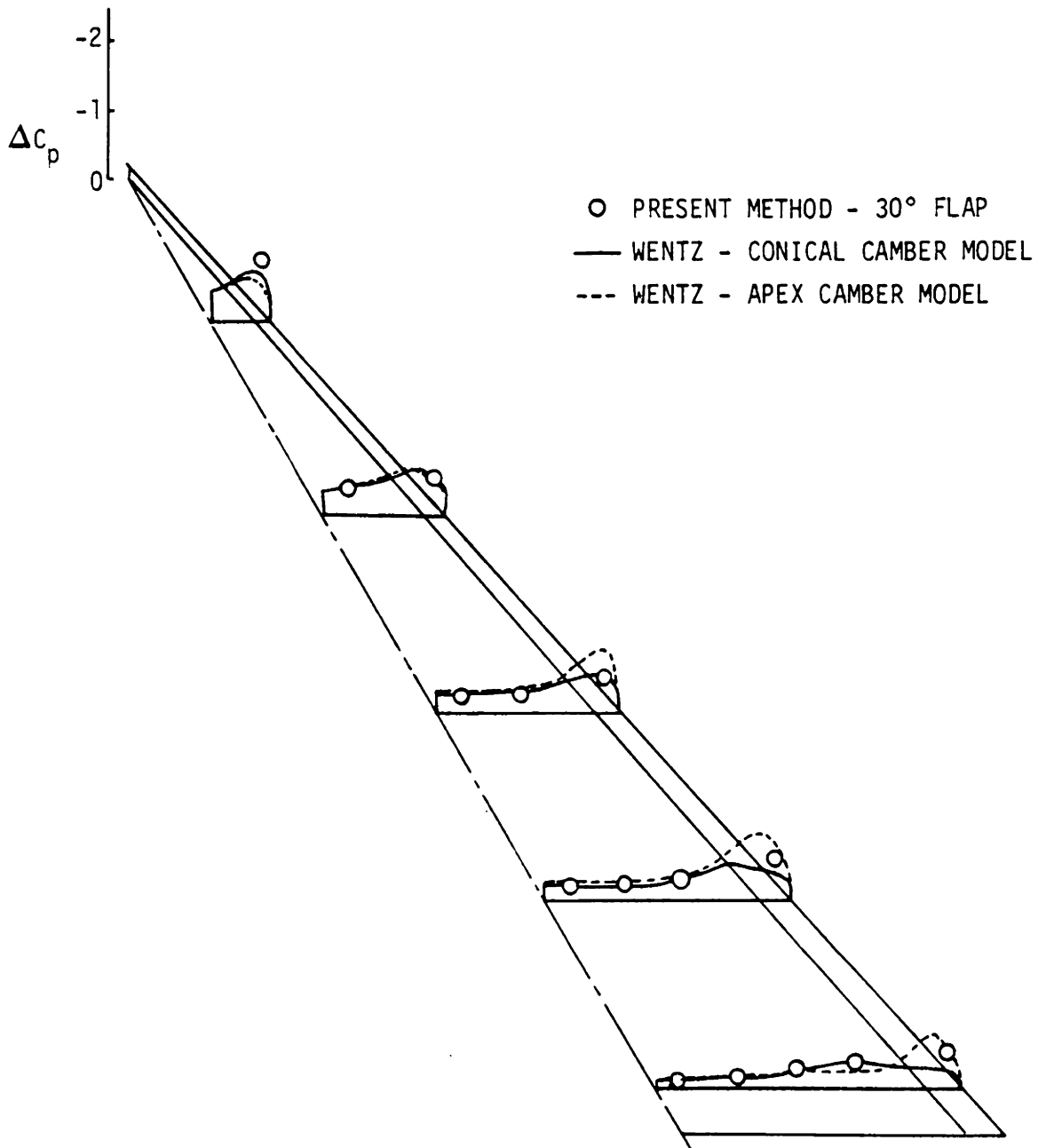


Figure 11. Pressure distribution - leading edge flap

$$\alpha = 10^\circ$$

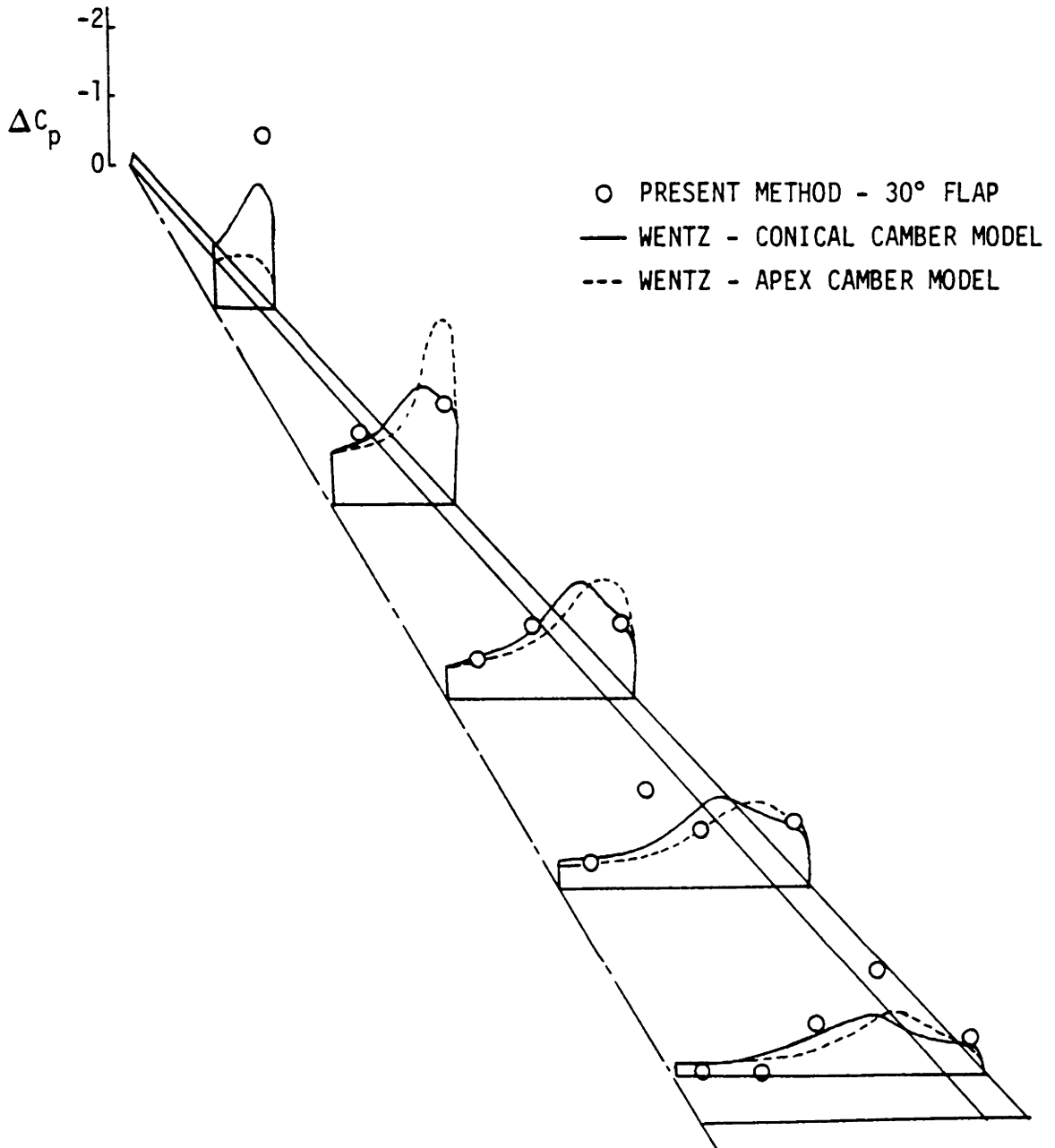


Figure 12. Pressure distribution - leading edge flap

$$\alpha = 20^\circ$$

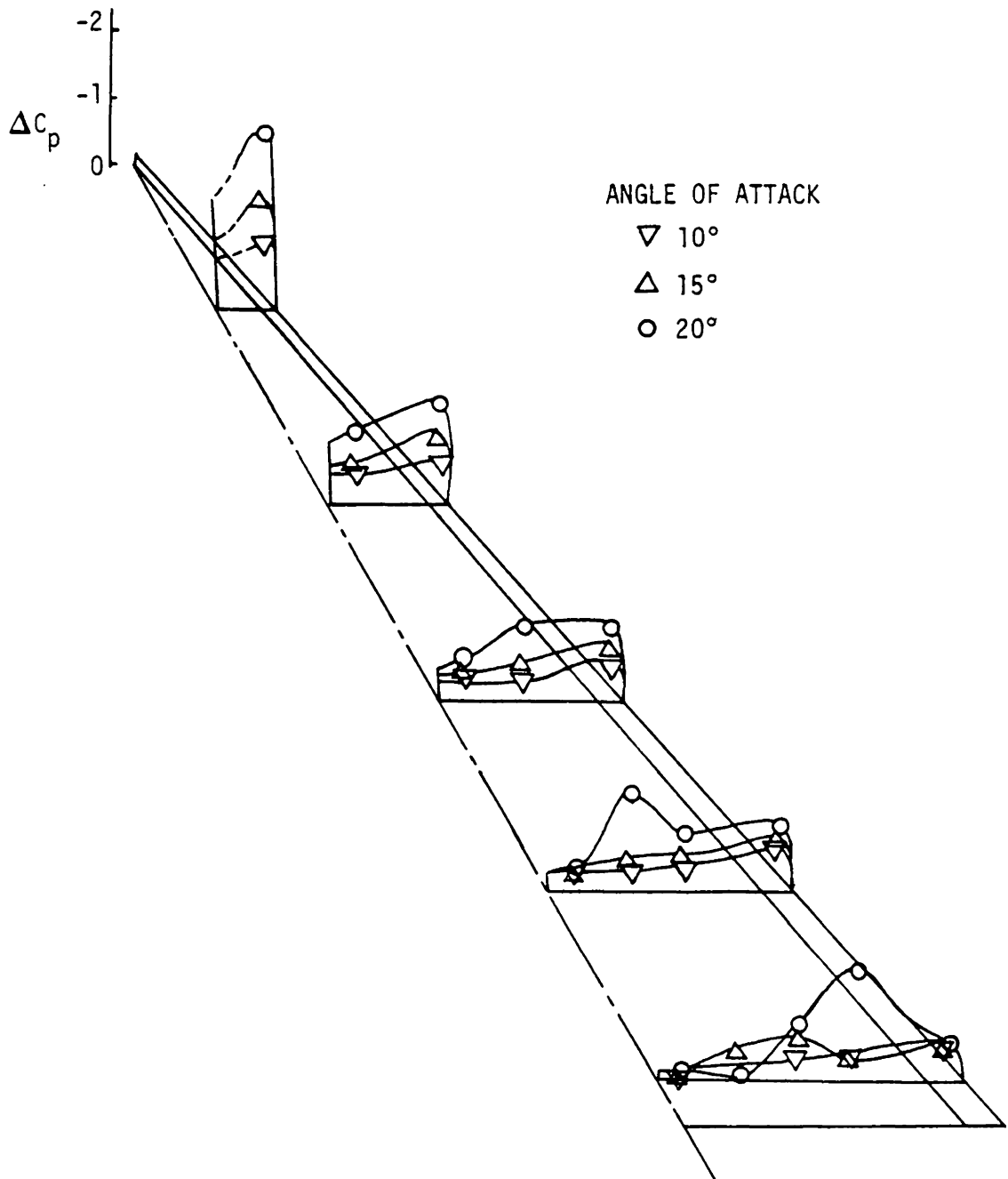
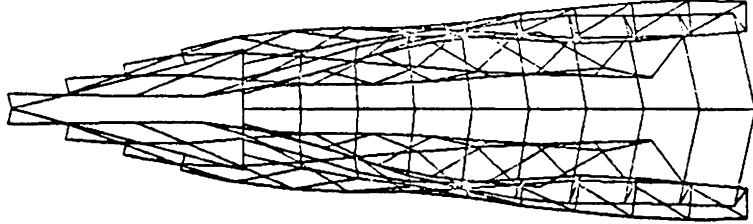


Figure 13. Pressure distribution - leading edge flap

TOP VIEW

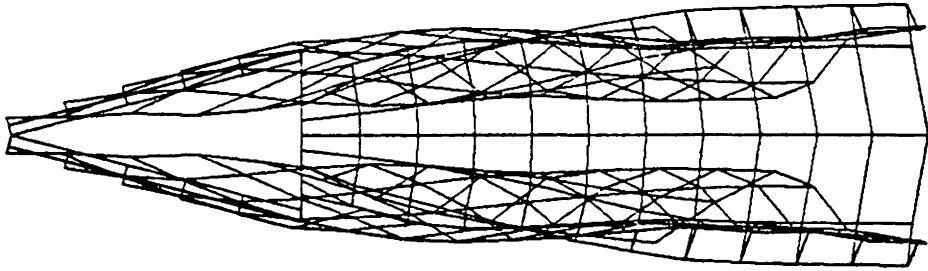


SIDE VIEW



Figure 14. Leading edge and trailing edge wakes
75° flat delta, angle of attack = 15°

TOP VIEW



SIDE VIEW

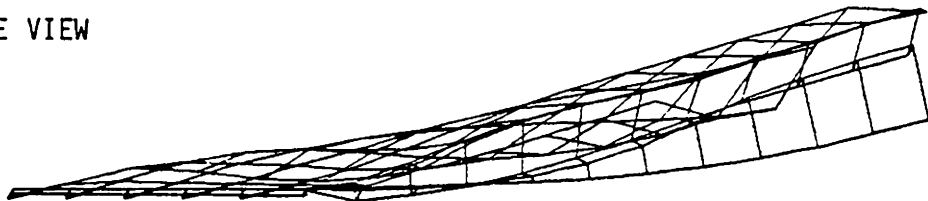


Figure 15. Leading edge and trailing edge wakes
75° delta with 30° leading edge flap
angle of attack = 15°

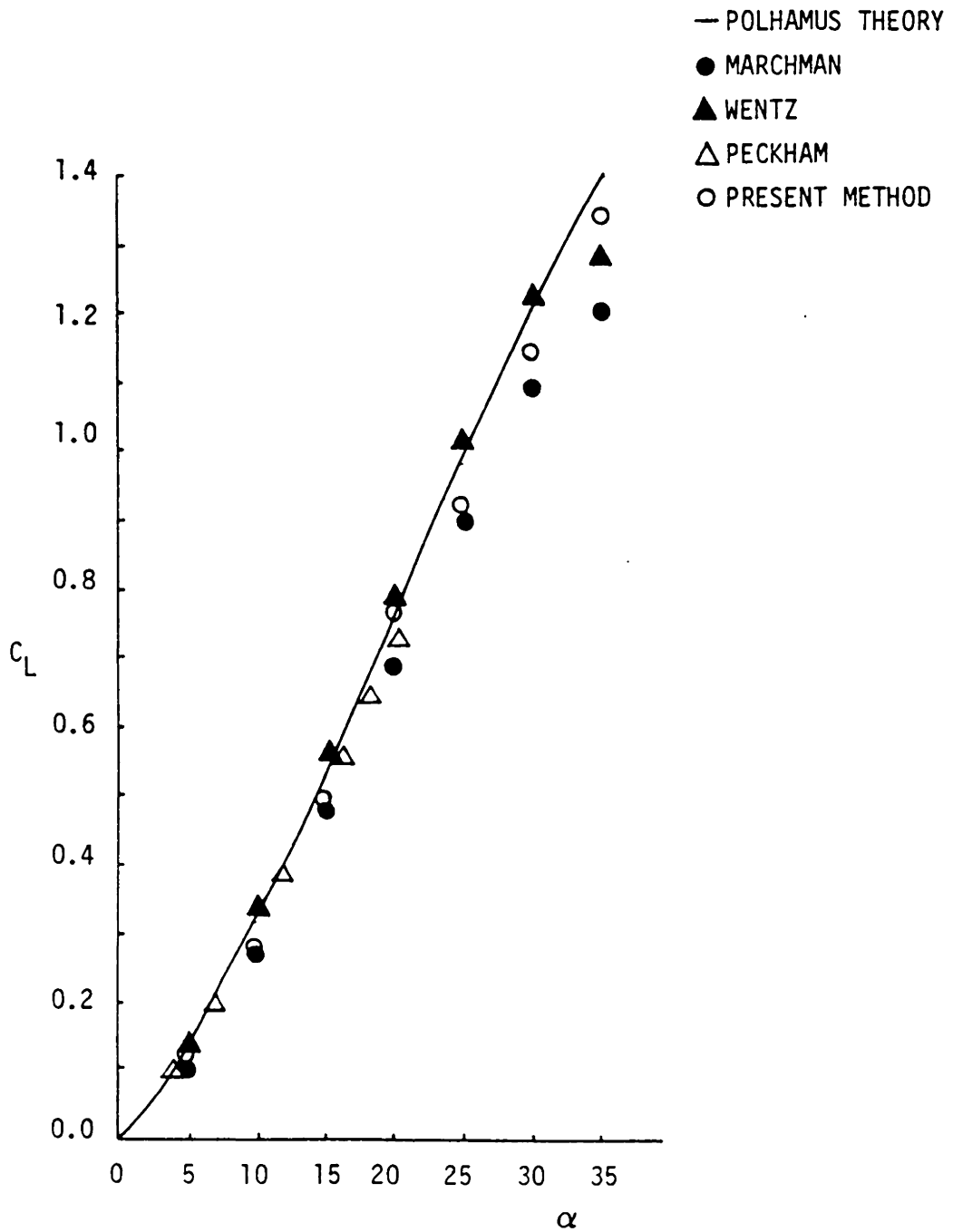


Figure 16. Lift coefficient vs angle of attack

No flap

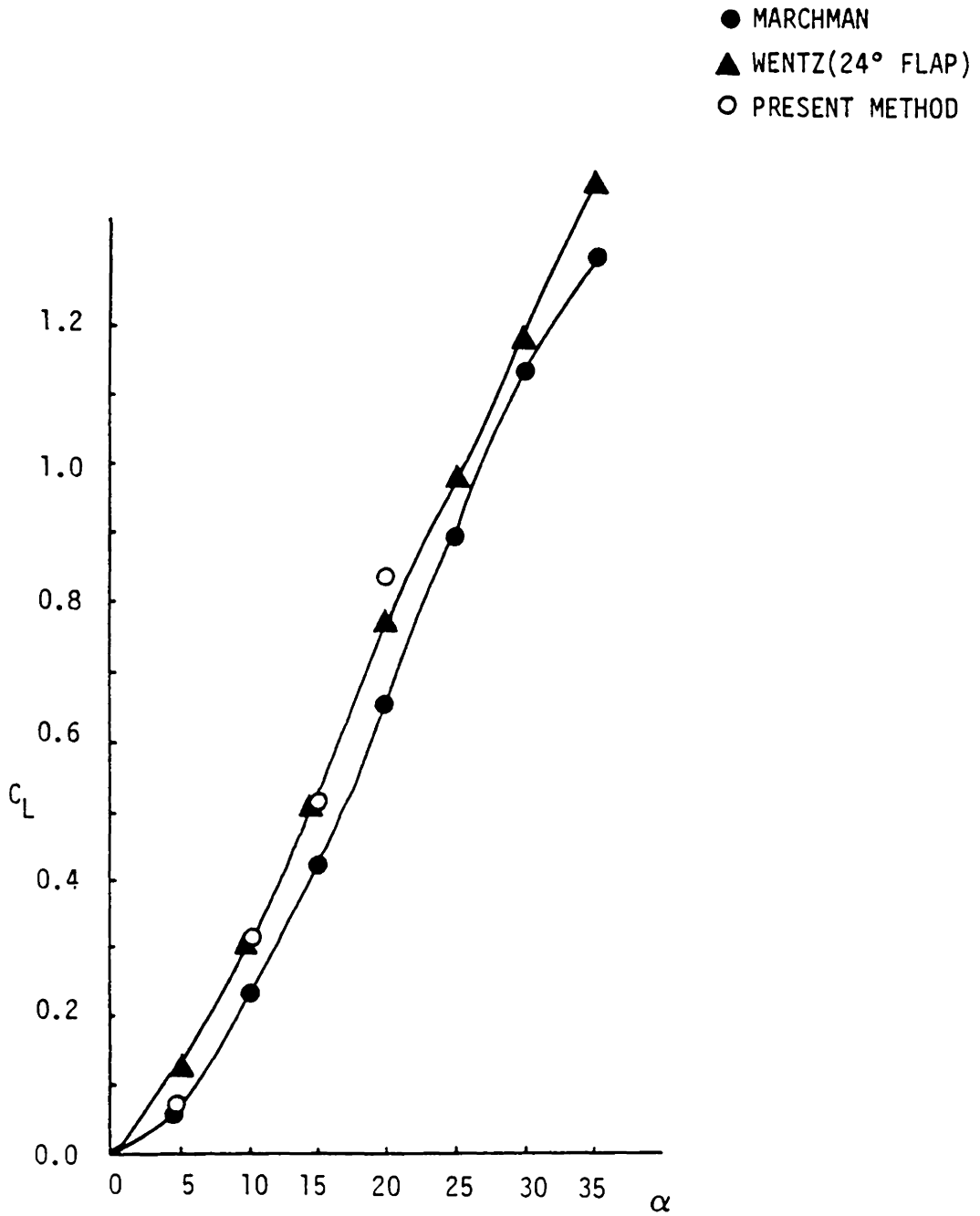


Figure 17. Lift coefficient vs angle of attack
30° leading edge flap

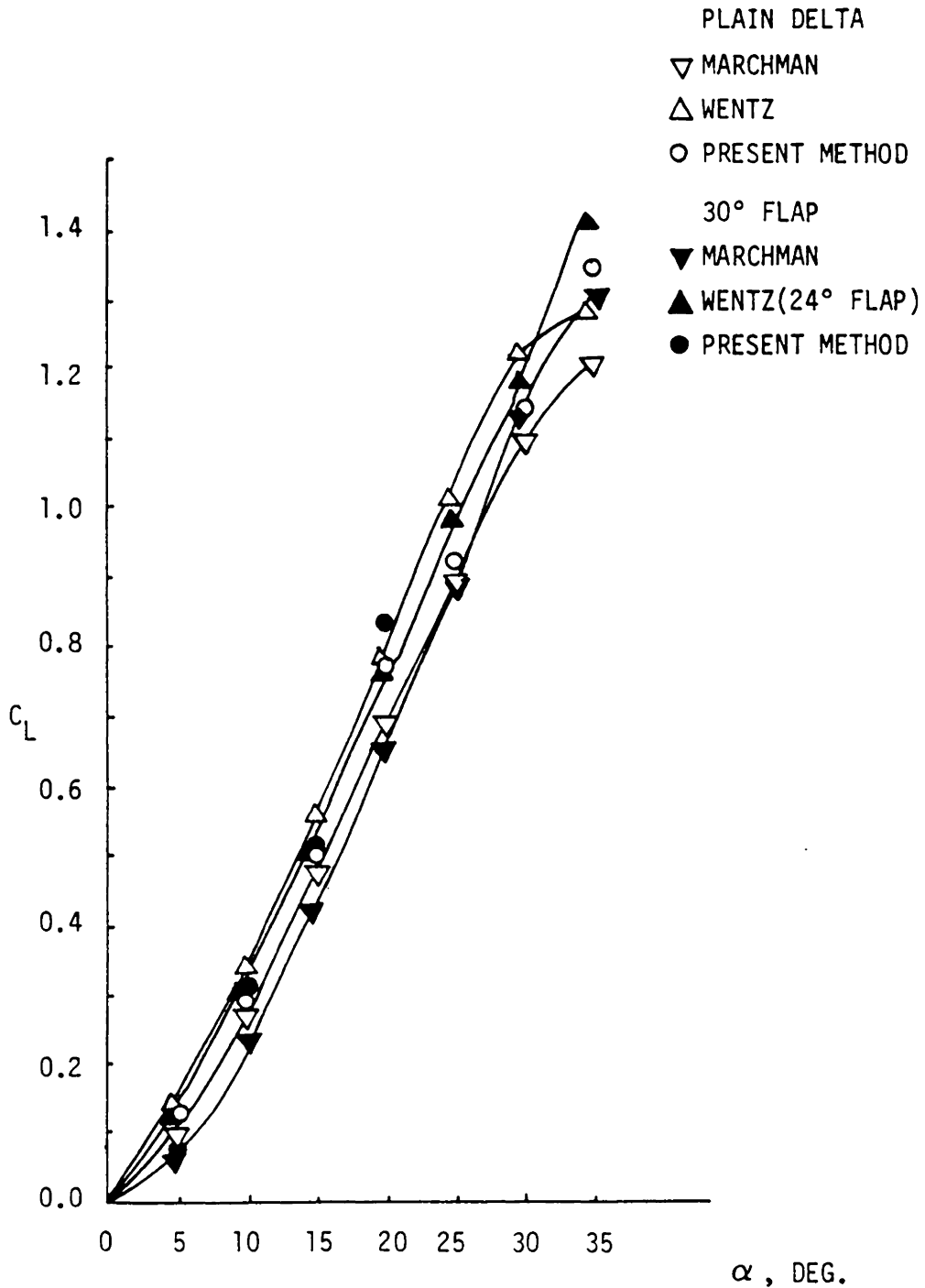


Figure 18. Lift coefficient vs angle of attack

Plain wing and leading edge flap

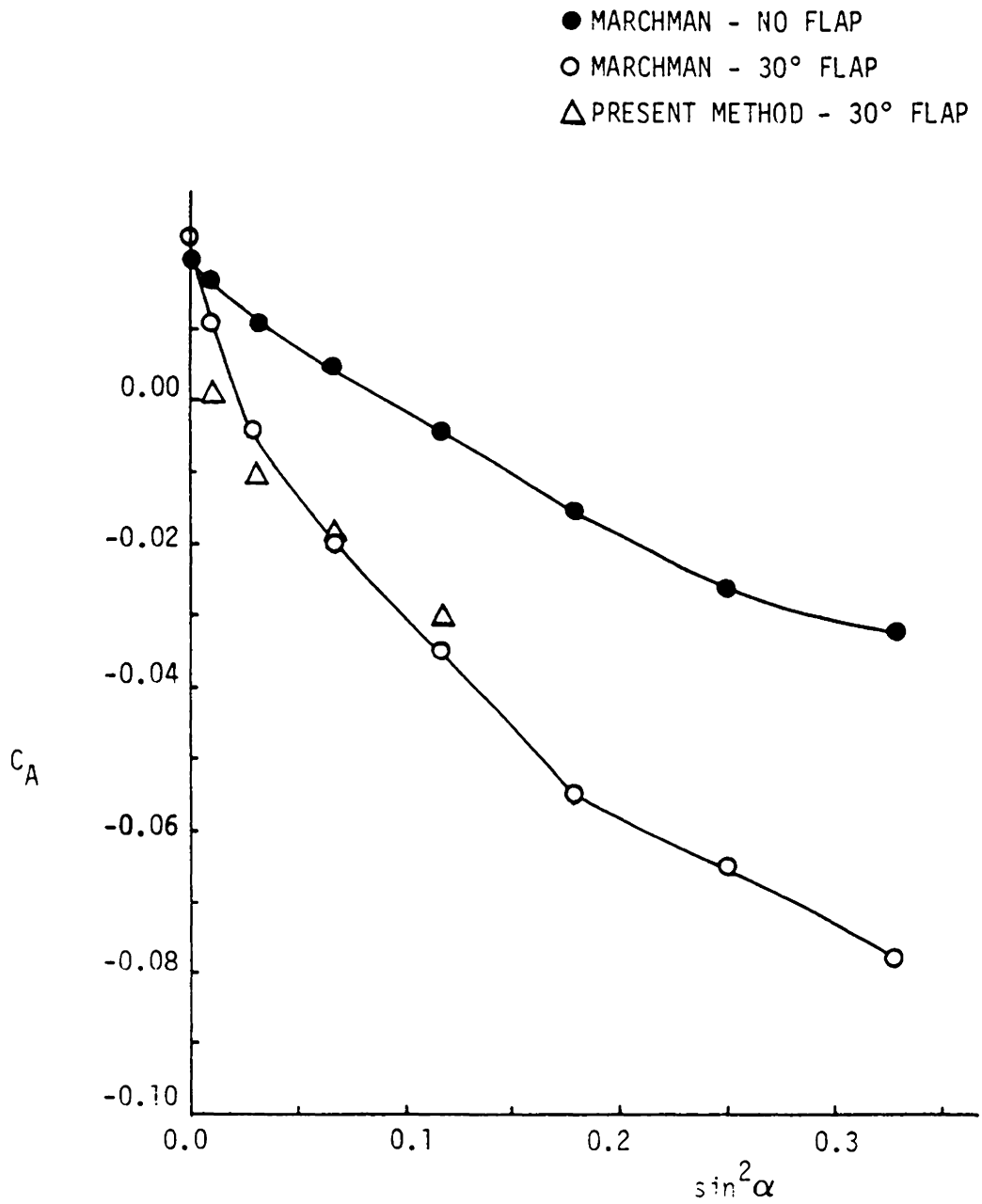


Figure 19. Axial force coefficient vs $\sin^2 \alpha$

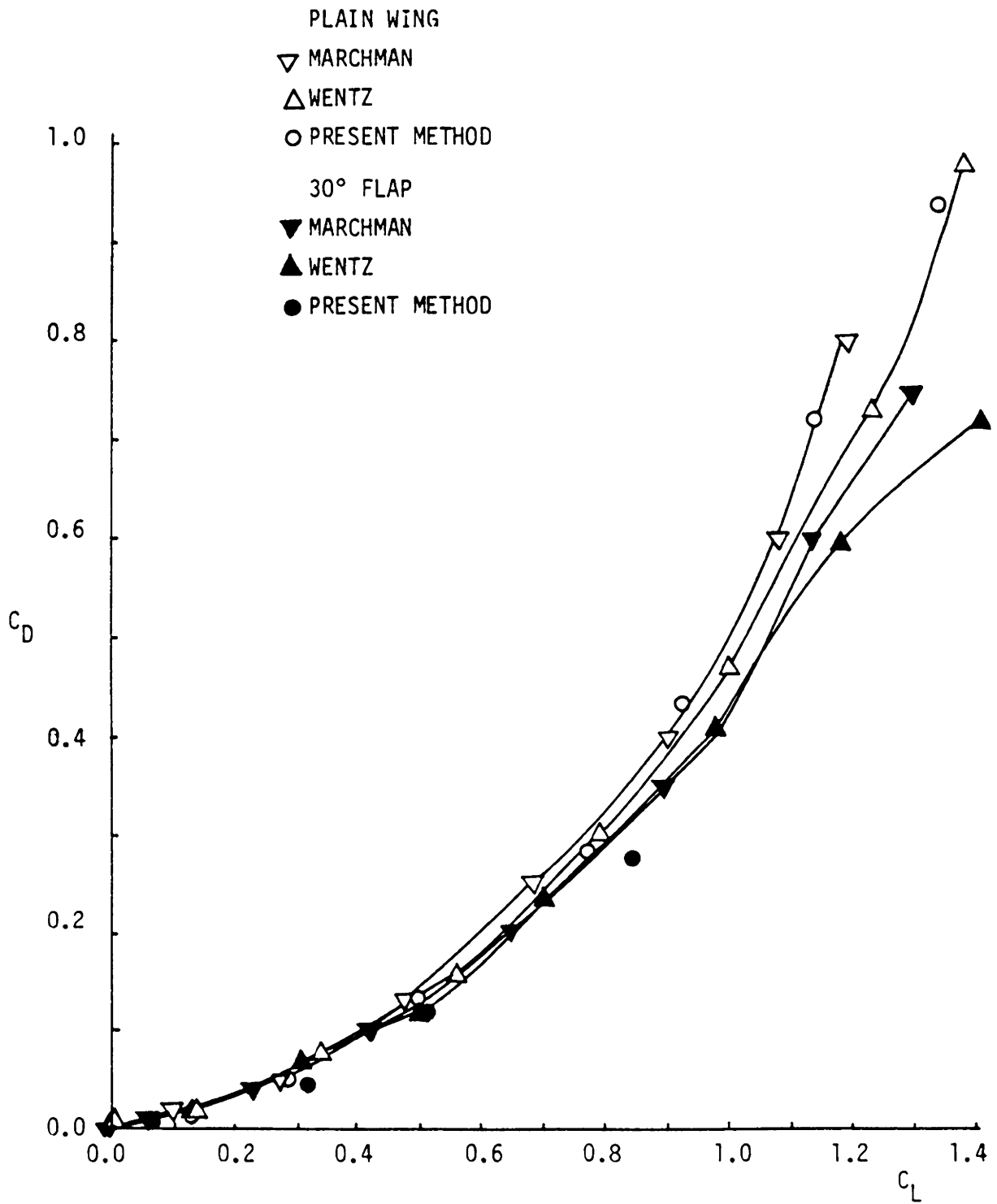


Figure 20. Drag coefficient vs lift coefficient

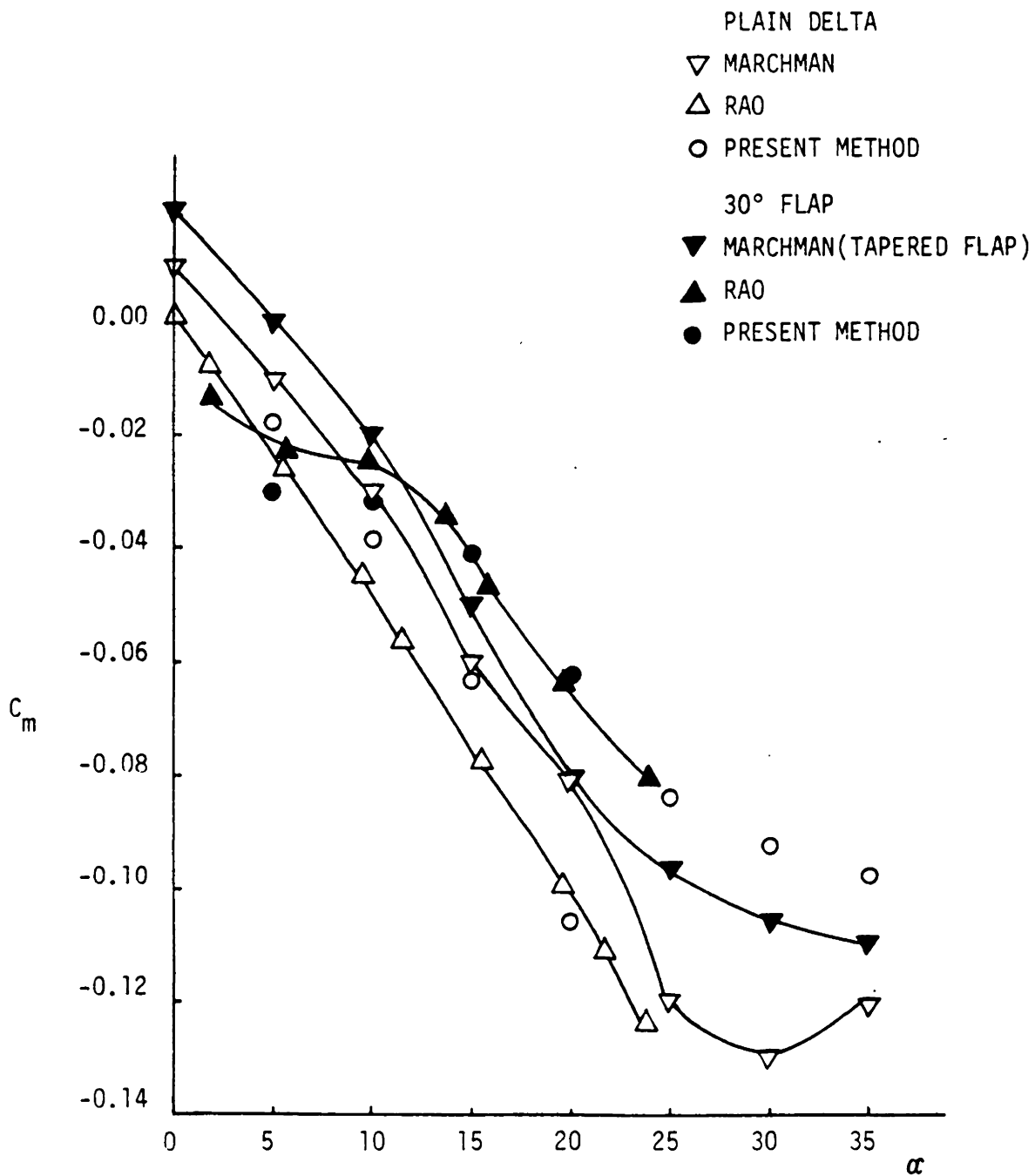


Figure 21. Pitching moment coefficient vs angle of attack
Moment about quarter mean aerodynamic chord

**The vita has been removed from
the scanned document**

A NUMERICAL STUDY OF THE EFFECTS OF LEADING EDGE
VORTEX FLAPS ON THE PERFORMANCE OF A 75° DELTA WING

by

Mary Ellen McNutt

(ABSTRACT)

Using a general, unsteady, nonlinear vortex lattice method, the aerodynamic loads have been found on a 75° delta wing with and without leading edge vortex flaps. The flap had an area approximately 26 percent of the wing area with a constant chord of 6.7 percent of the wing mean aerodynamic chord and was deflected at 30°.

Results for lift, drag, axial force, and pitching moment coefficients are compared with experimental data and show very good agreement. Individual pressure difference coefficients along the wing and flap are also presented and compared with experimental data.

Overall, the method shows the leading edge vortex flap to be very effective in reducing drag while maintaining lift comparable to that of the plain wing.